Supporting Information for

Alkyl Yttrium Complexes of Amidine-amidopyridinate Ligands. Intramolecular C(sp3)–H Activation and Reactivity Studies.

Vasily Rad'kov,[a,c] Vincent Dorcet,[b] Jean-François Carpentier,[a*] Alexander Trifonov,[c*] and Evgeny Kirillov [a*]

[a] *Organometallics: Materials and Catalysis, Institut des Sciences Chimiques de Rennes, UMR 6226 CNRS – Université de Rennes 1, Rennes, France*

[b] *Centre de Diffractométrie X, Institut des Sciences Chimiques de Rennes, UMR 6226 CNRS – Université de Rennes 1, Rennes, France*

[c] *G. A. Razuvaev Institute of Organometallic Chemistry of RAS, Nizhny Novgorod, Russia*

Figure S9. $^{13}C\{^1H\}$ NMR spectrum (125 MHz, C_6D_6, 298 K) of $\{N^{Me2}NN^{Me2}C^{Me}N^{Me2}\}Y(CH_2C_6H_4\text{-}o\text{-}NMe_2)_2$ (2b).

Figure S10. ^1H NMR spectrum (400 MHz, toluene-d_8, 233 K) of the reaction product (3) of 2a' with 1 equiv of $B(C_6F_5)_3$.

Figure S11. ^1H–^1H COSY spectrum (400 MHz, toluene-d_8, 233 K) of the reaction product (3) of 2a' with 1 equiv of $B(C_6F_5)_3$.

Figure S12. $^{19}F\{^1H\}$ NMR spectrum (376 MHz, toluene-d_8, 233 K) of the reaction product (3) of 2a' with 1 equiv of $B(C_6F_5)_3$.

Figure S13. ^{13}C DEPT 135 NMR spectrum (100 MHz, toluene-d_8, 233 K) of the reaction product (3) of 2a' with 1 equiv of $B(C_6F_5)_3$.

Figure S14. ^1H NMR spectrum (400 MHz, THF-d_8, 273 K) of the reaction product (4) of 2a' with 1 equiv of $[HNEt_3]^+[BPh_4]^-$.

Figure S15. ^{13}C DEPT 135 NMR spectrum (400 MHz, THF-d_8, 273 K) of the reaction product (4) of 2a' with 1 equiv of $[HNEt_3]^+[BPh_4]^-$.

Figure S16. ^1H NMR spectrum (500 MHz, C_6D_6, 298 K) of the reaction product (5) of 2a' with 1 equiv of *i*PrN=C(PPh_2)-N(H)*i*Pr.

Figure S17. $^{13}C\{^1H\}$ NMR spectrum (125 MHz, C_6D_6, 298 K) of the reaction product (5) of 2a' with 1 equiv of *i*PrN=C(PPh_2)-N(H)*i*Pr.

Figure S18. $^{31}P\{^1H\}$ NMR spectrum (121.5 MHz, C_6D_6, 298 K) of the reaction product (5) of 2a' with 1 equiv of *i*PrN=C(PPh_2)-N(H)*i*Pr.

Figure S19. ^1H NMR spectrum (500 MHz, toluene-d_8, 298 K) of the reaction product (6) of 2a' with 1 equiv of NH_3BH_3.

Figure S20. ^1H NMR spectrum (500 MHz, toluene-d_8, 333 K) of $[\{N^{Me2}NN^{Me2}C^{Me}N^{Me}\text{–}CH_2(\mu\text{-}O)\}Y(CH_2SiMe_3)]_2$ (7).

Table S1. Summary of crystal and refinement data for compounds 1, **2a'**, 6 and 7.

Table S2. Experimental (DRX) and calculated (M06, B3LYP) geometrical parameters and Wiberg bond indexes for 1 and **2a'**.

Figure S21. Kohn-Sham orbitals of **2a'** determined from M06 level calculations (isosurface value, 0.03): (a) HOMO (–0.1724 a.u.), (b) HOMO–1 (–0.1917 a.u.).

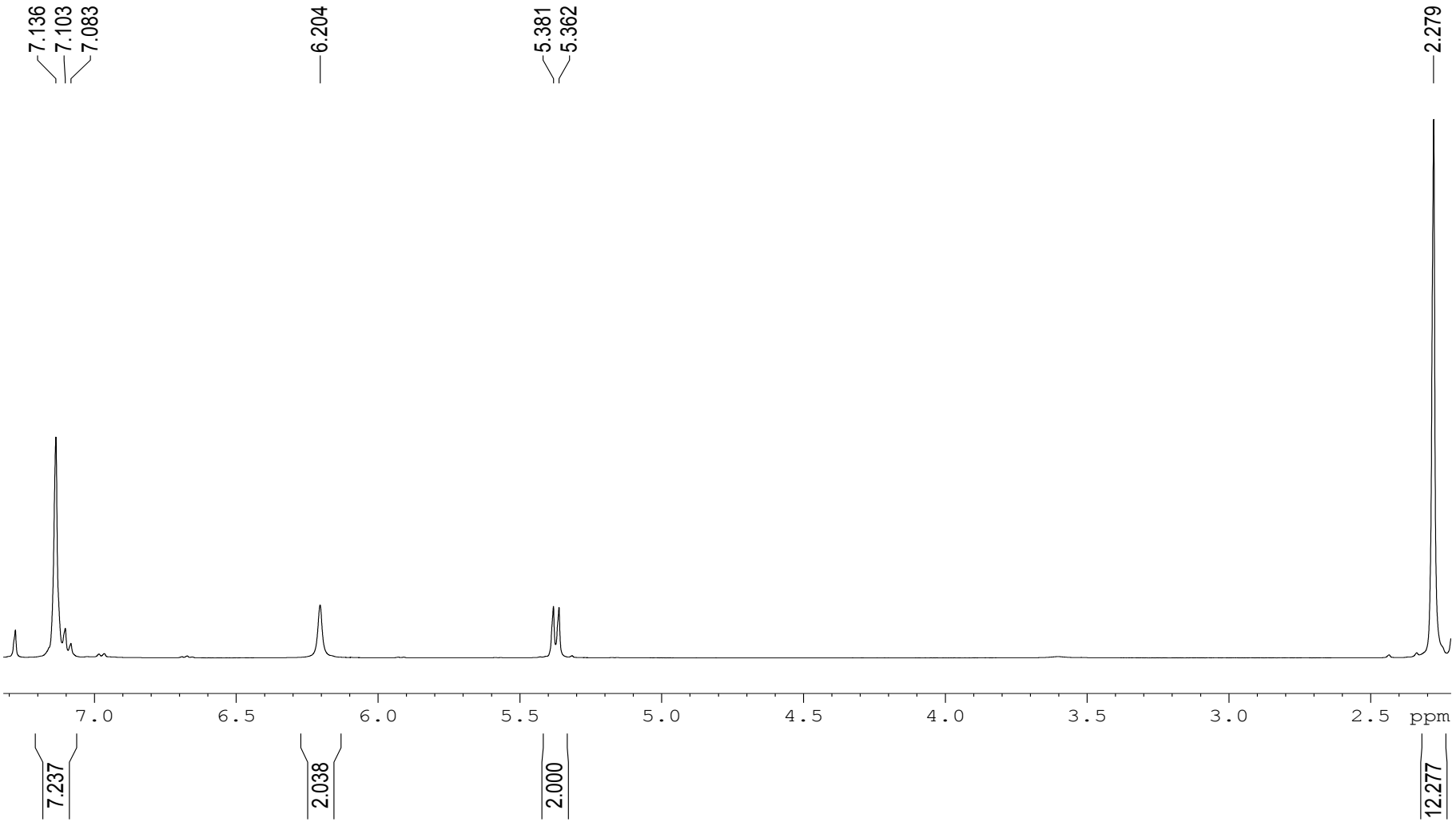

Figure S1. ^{1}H NMR spectrum (400 MHz, $CDCl_3$, 298 K) of $(N^{Me2}NN^{Me2})H_2$.

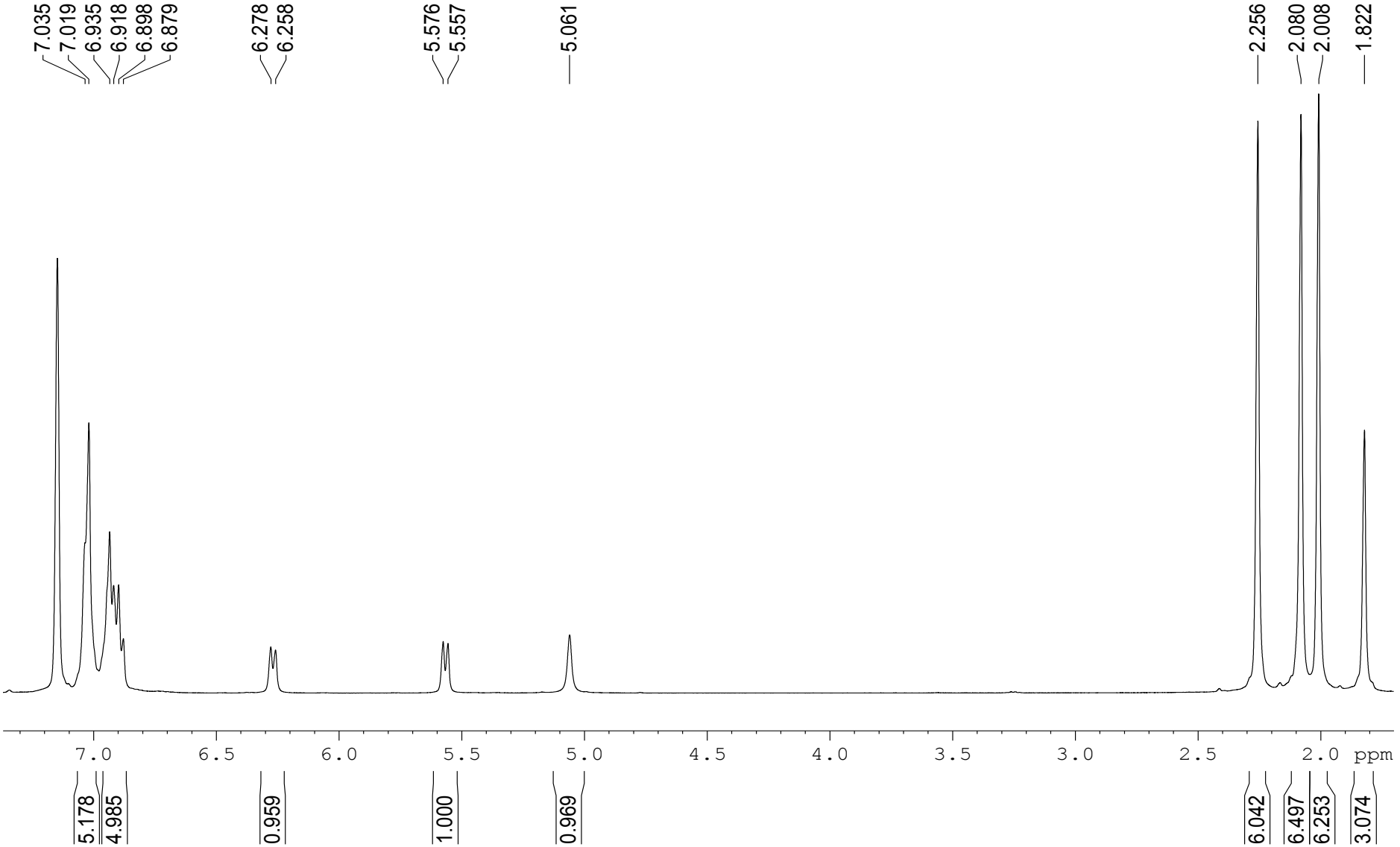

Figure S2. ^{1}H NMR spectrum (400 MHz, C_6D_6, 298 K) of $\{N^{Me2}NN^{Me2}C^{Me}N^{Me2}\}H$ (1).

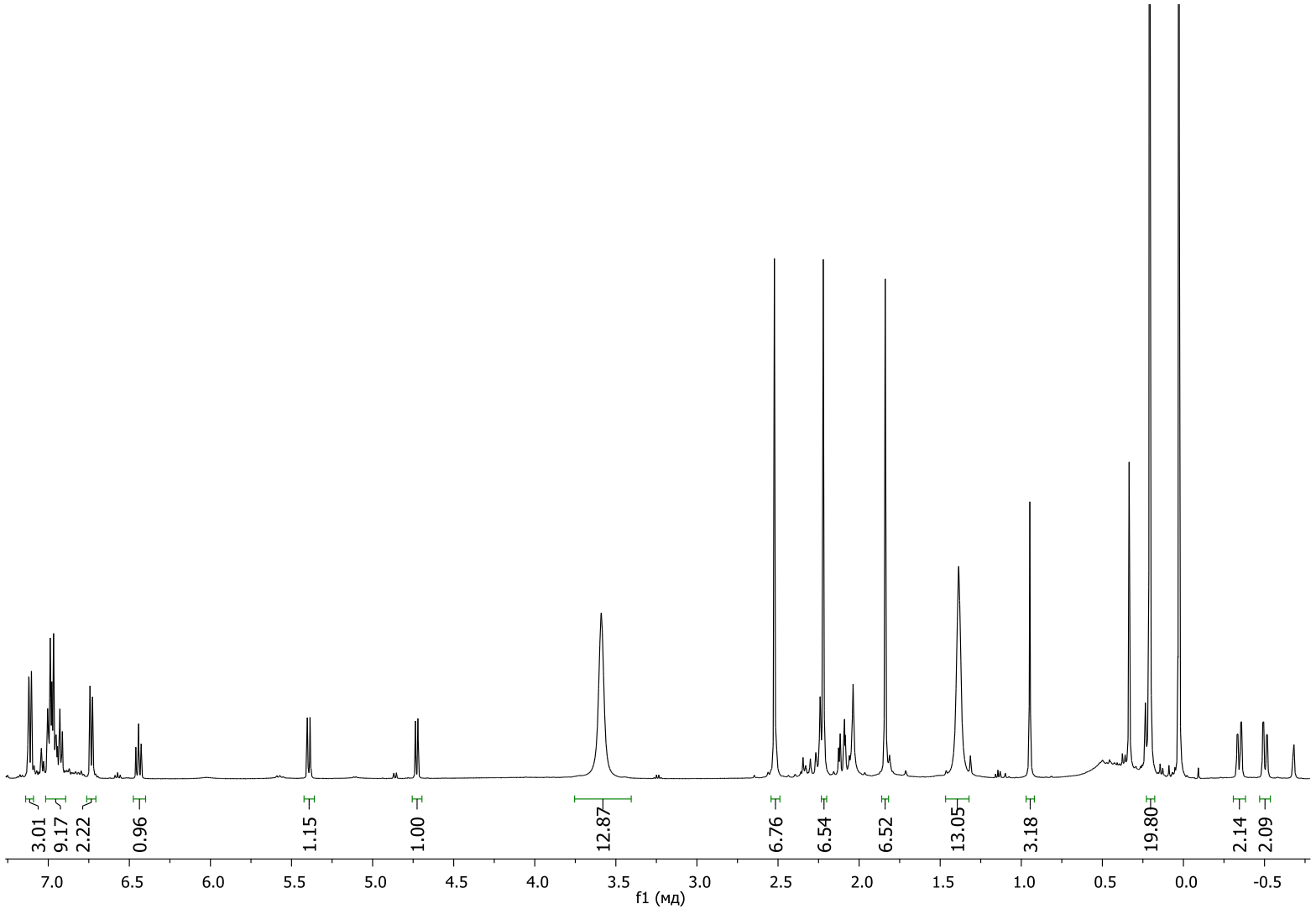

Figure S3. ^{1}H NMR spectrum (500 MHz, toluene-d_8, 243 K) of the reaction product (2a) of 1 with 1 equiv of $Y(CH_2SiMe_3)_3(THF)_2$.

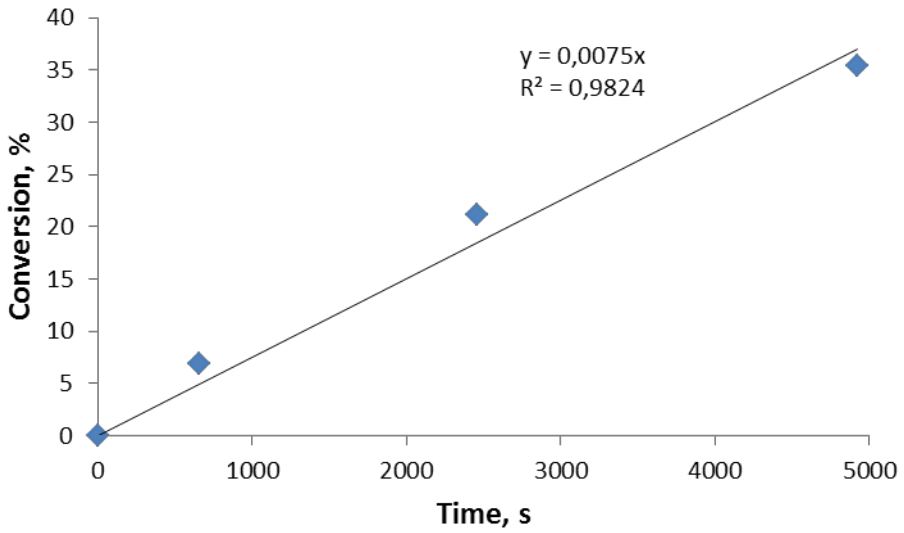

Figure S4. Kinetic data (conversion (%) vs. time (s)) for the intramolecular C–H bond activation reaction in the alkyl complex **2a**, monitored in toluene-d_8 at –30 °C.

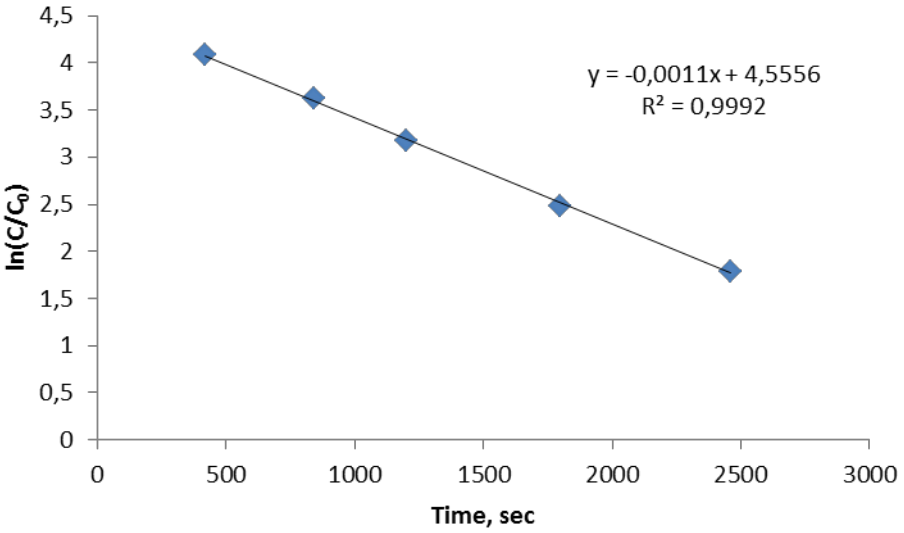

Figure S5. Kinetic data ($\ln(C/C_0)$ *vs.* time (s)) for the reaction of alkyl complex **2a'** with 1 equiv of $[Et_3NH][BPh_4]$, monitored in THF-d_8 at –10 °C.

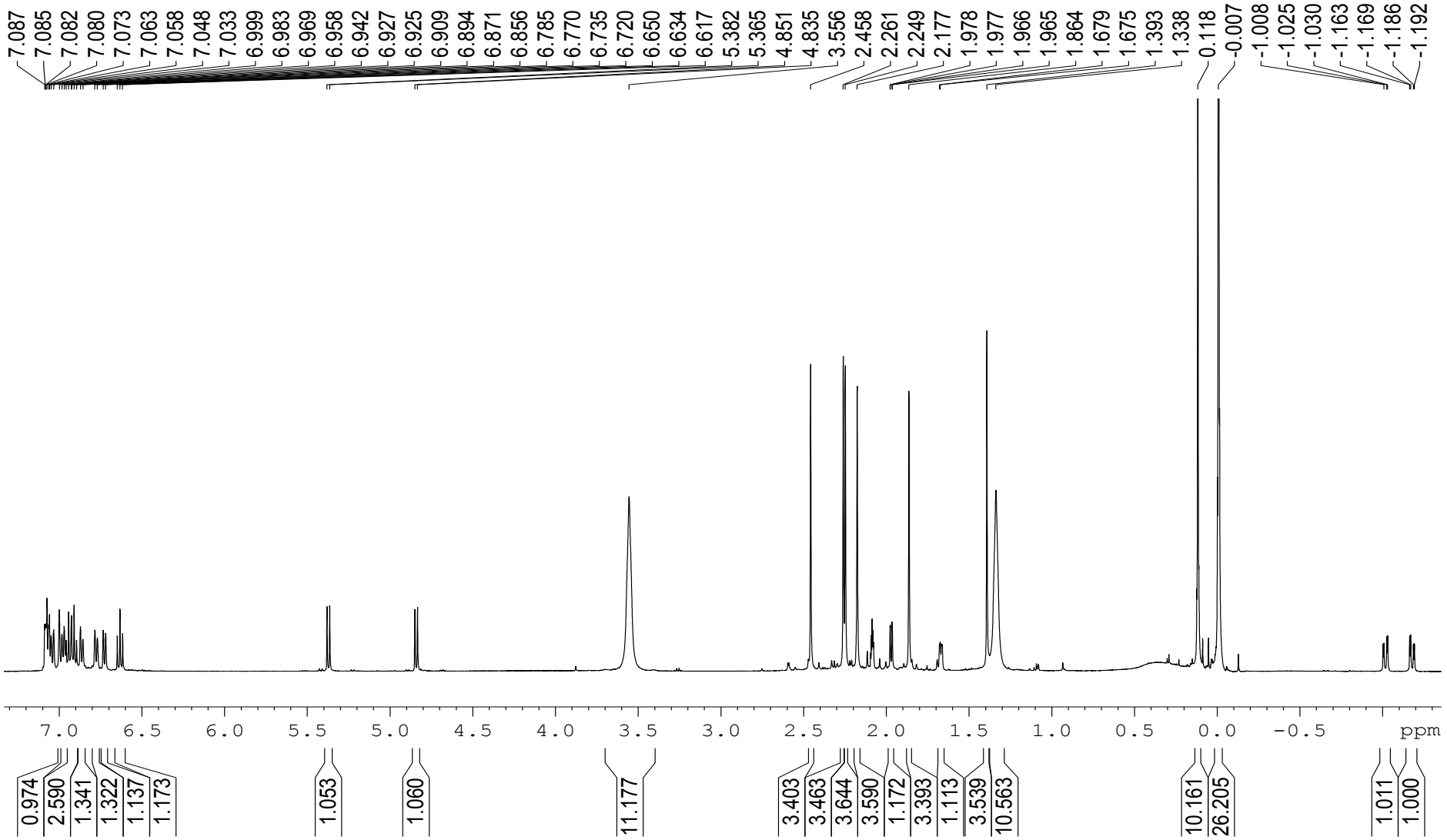

Figure S6. ^{1}H NMR spectrum (500 MHz, toluene-d_8, 298 K) of {N^{Me2}NN^{Me2}C^{Me}N^{Me}–CH_2}Y(CH_2SiMe_3)(THF) (**2a'**).

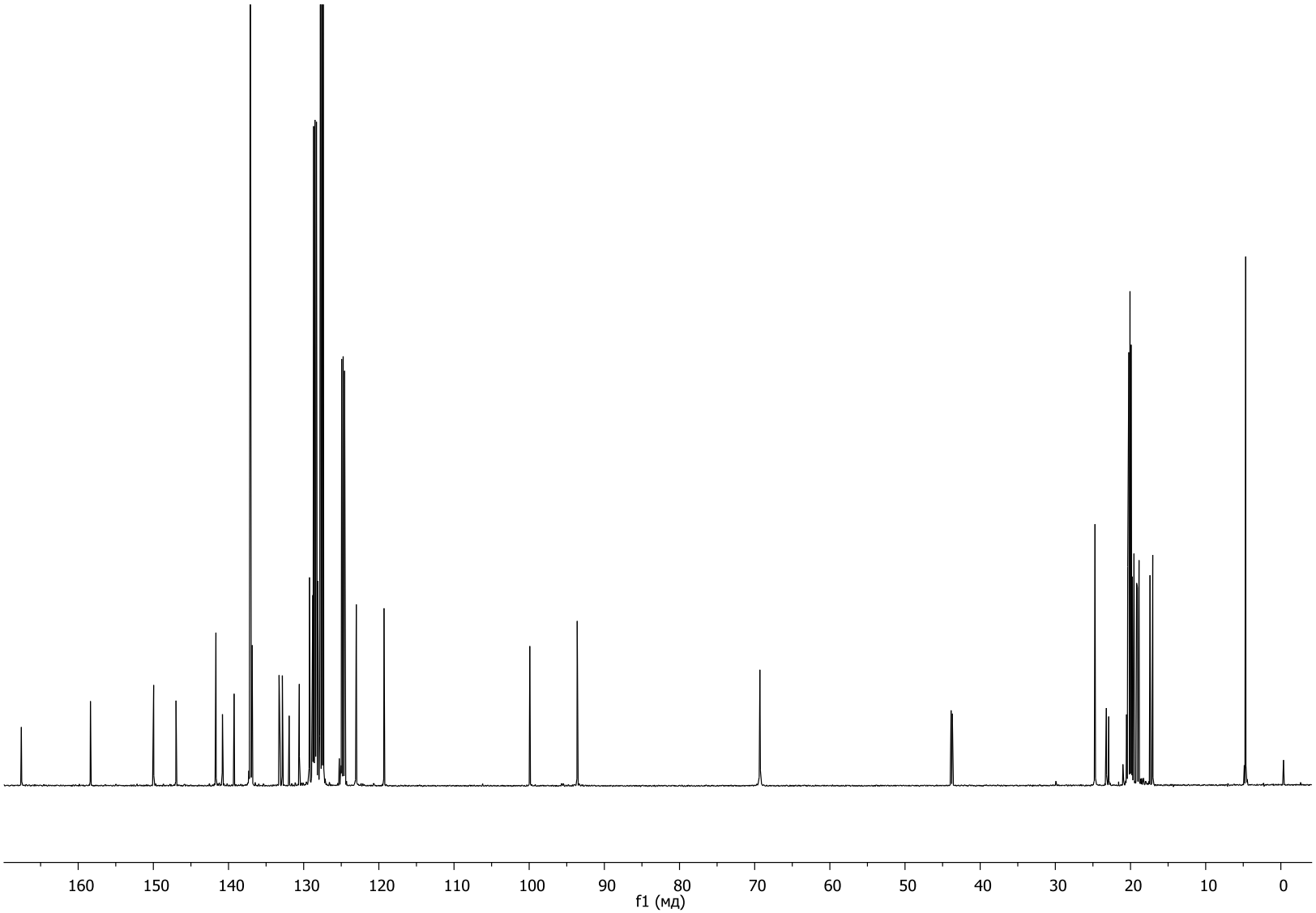

Figure S7. $^{13}C\{^{1}H\}$ NMR spectrum (125 MHz, toluene-d_8, 298 K) of $\{N^{Me2}NN^{Me2}C^{Me}N^{Me}\text{–}CH_2\}Y(CH_2SiMe_3)(THF)$ (2a').

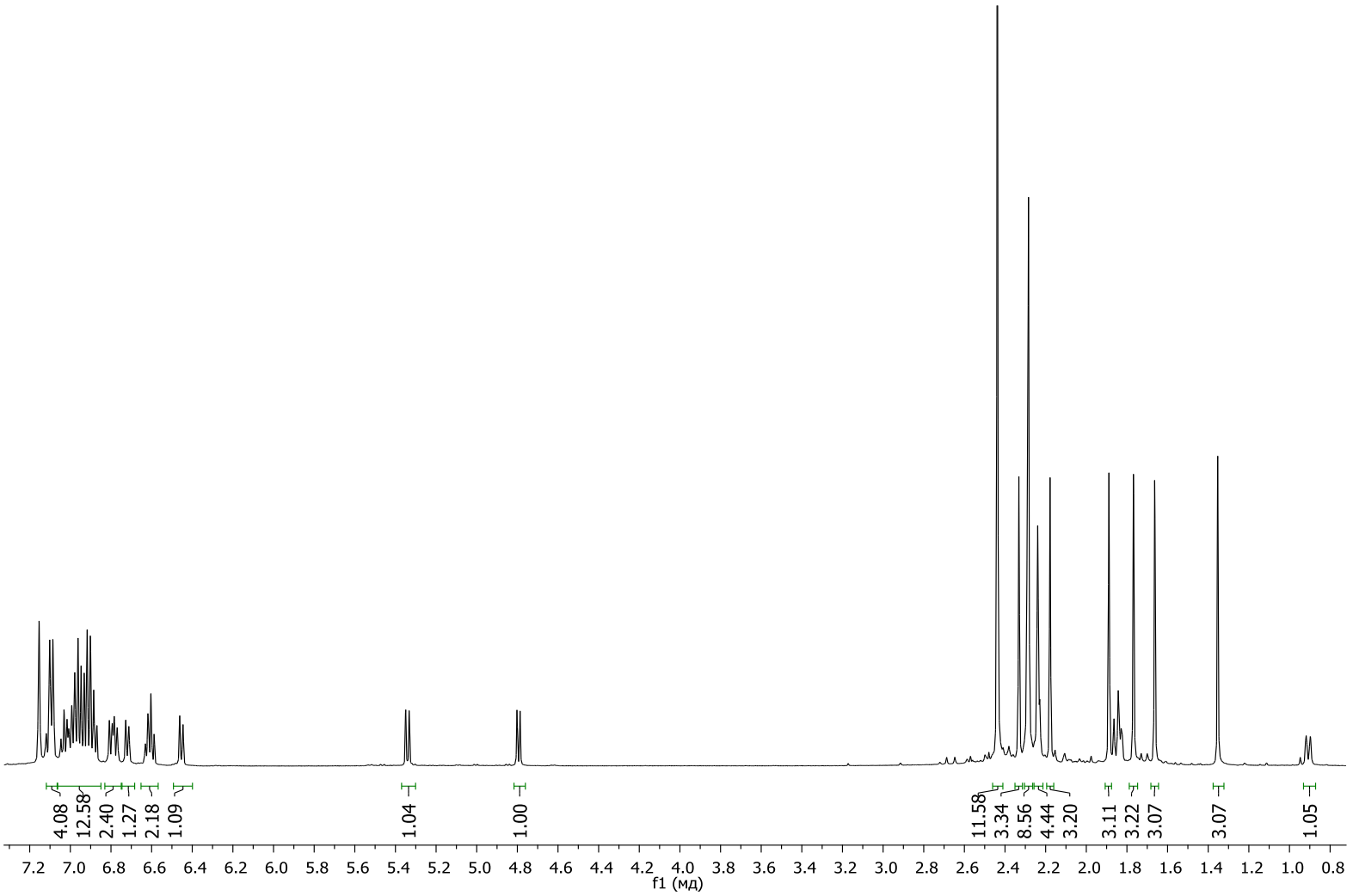

Figure S8. ^{1}H NMR spectrum (500 MHz, C_6D_6, 298 K) of $\{N^{Me2}NN^{Me2}C^{Me}N^{Me2}\}Y(CH_2C_6H_4\text{-}o\text{-}NMe_2)_2$ (2b).

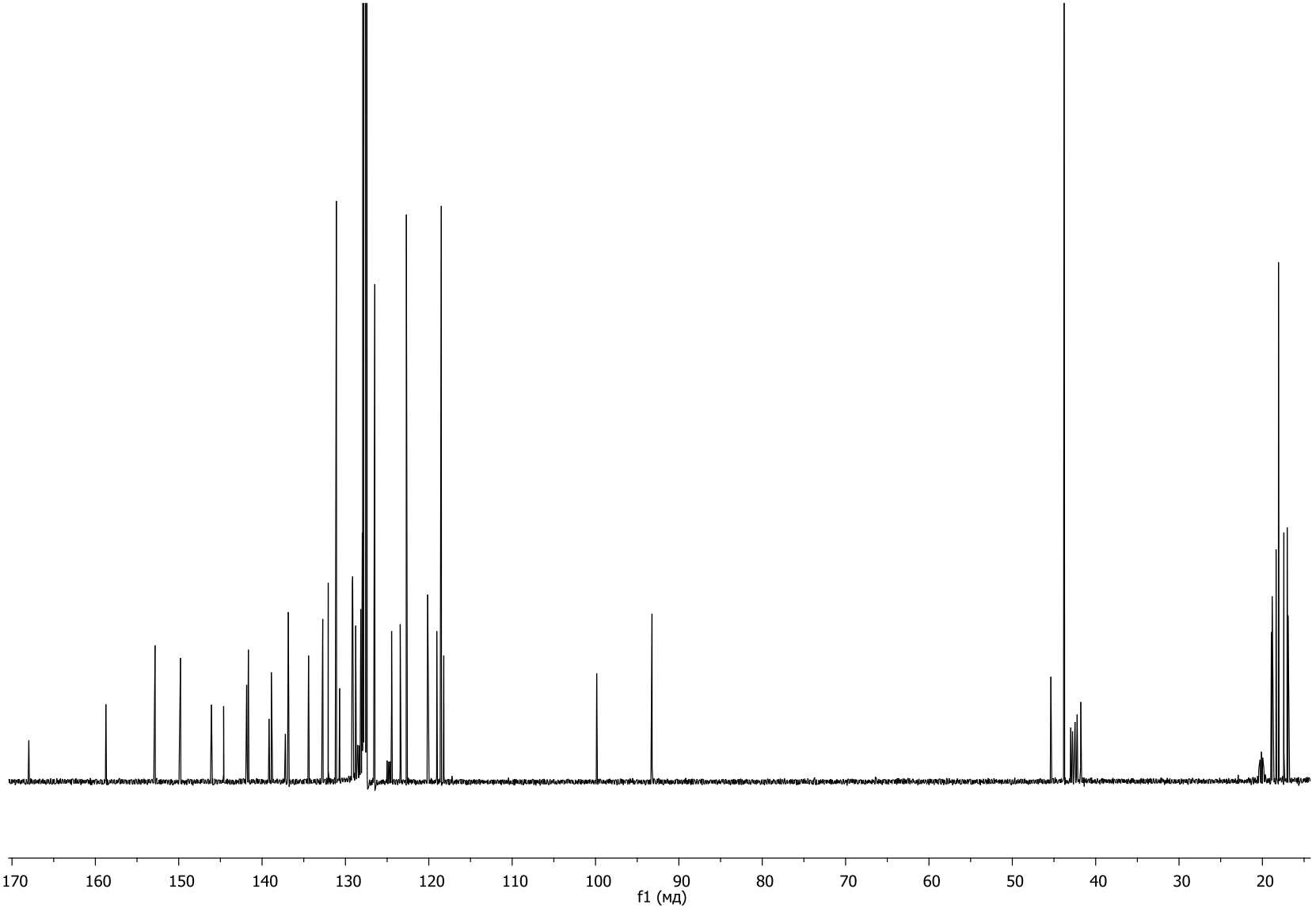

Figure S9. $^{13}C\{^{1}H\}$ NMR spectrum (125 MHz, C_6D_6, 298 K) of $\{N^{Me2}NN^{Me2}C^{Me}N^{Me2}\}Y(CH_2C_6H_4\text{-}o\text{-}NMe_2)_2$ (2b).

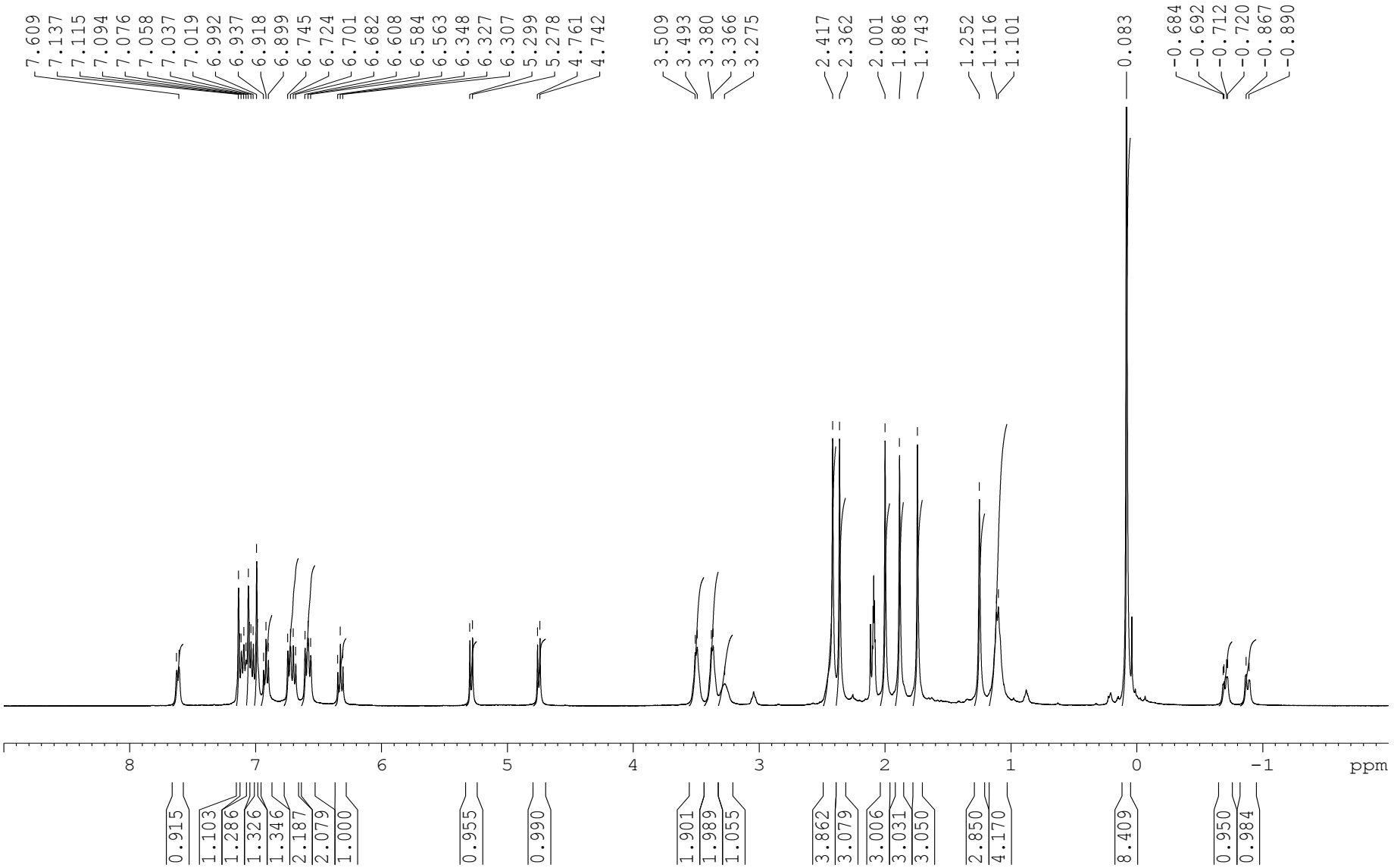

Figure S10. ^{1}H NMR spectrum (400 MHz, toluene-d_8, 233 K) of the reaction product (3) of 2a' with 1 equiv of $B(C_6F_5)_3$.

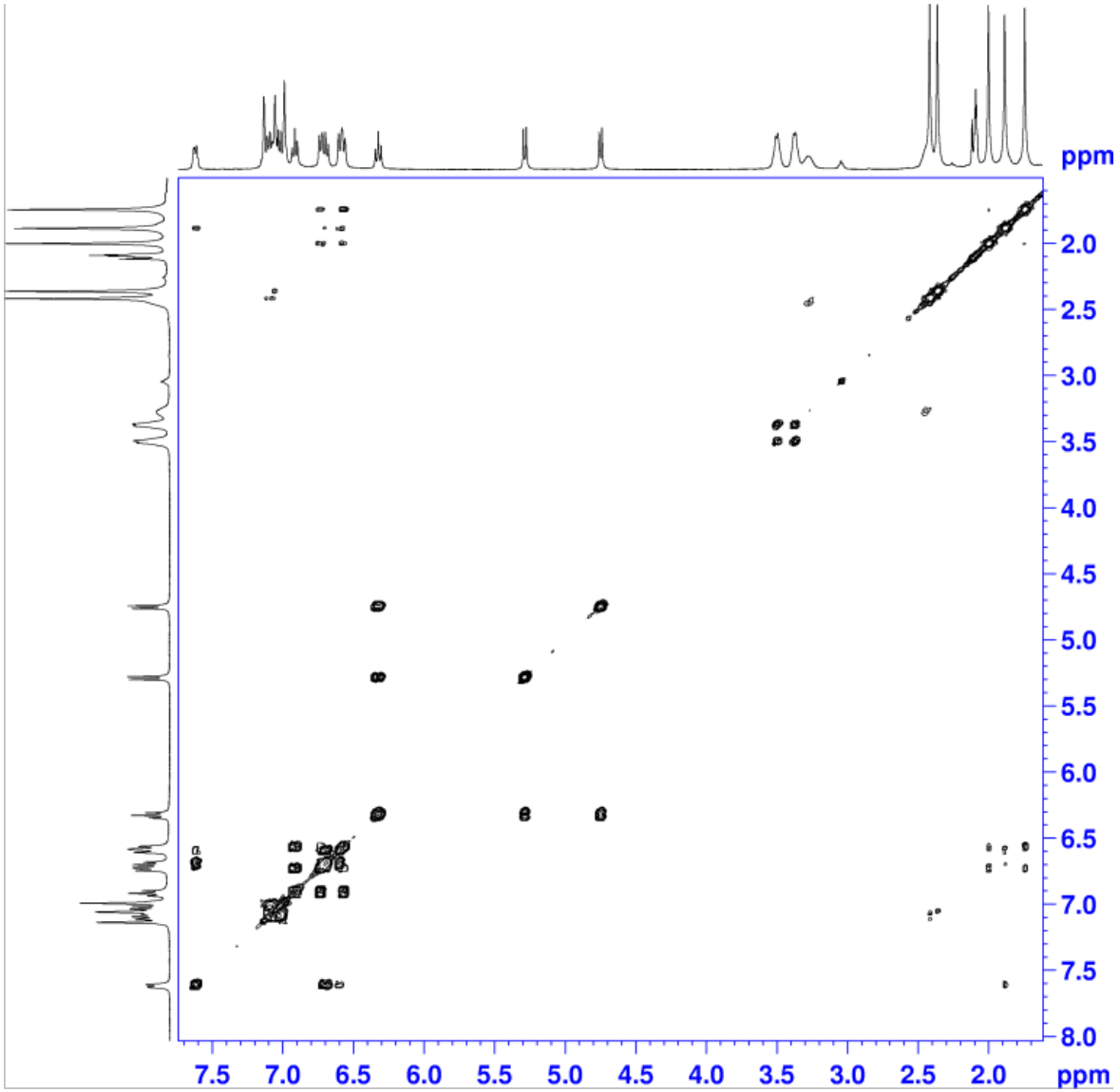

Figure S11. ^{1}H–^{1}H COSY spectrum (400 MHz, toluene-d_8, 233 K) of the reaction product (3) of **2a'** with 1 equiv of $B(C_6F_5)_3$.

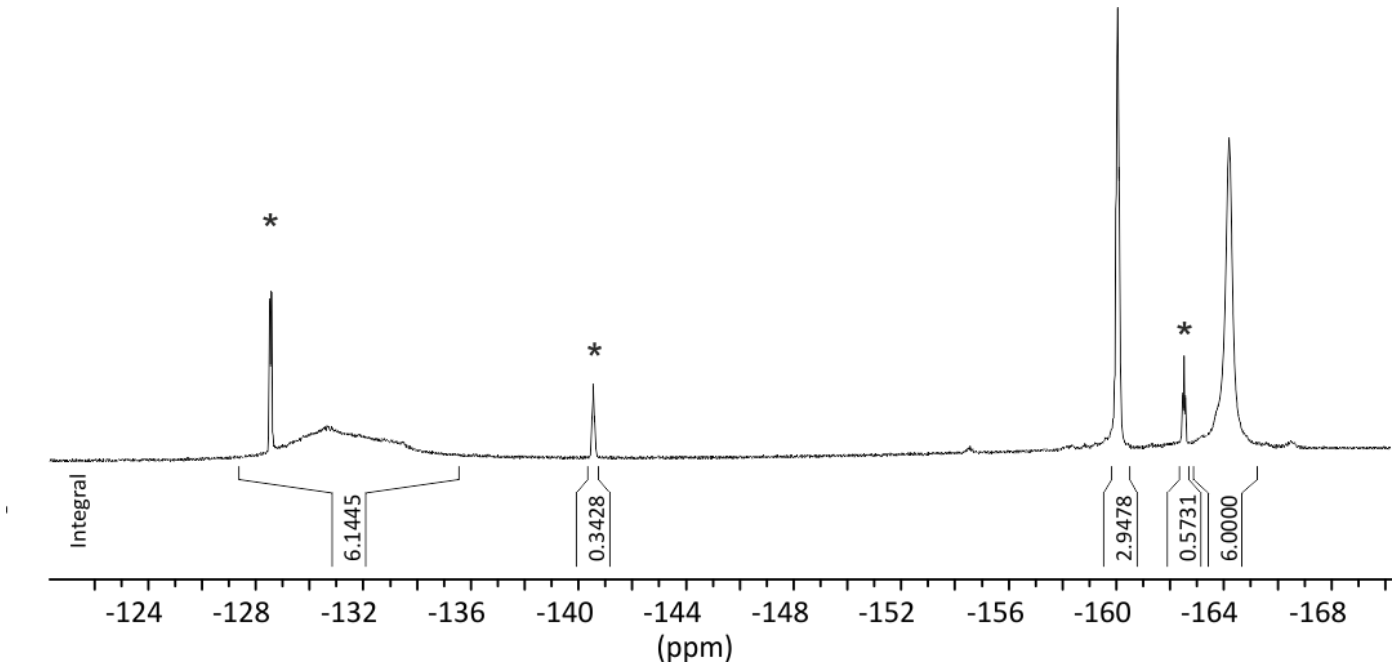

Figure S12. $^{19}F\{^{1}H\}$ NMR spectrum (376 MHz, toluene-d_8, 233 K) of the reaction product (3) of 2a' with 1 equiv of $B(C_6F_5)_3$. * stand for excess of $B(C_6F_5)_3$.

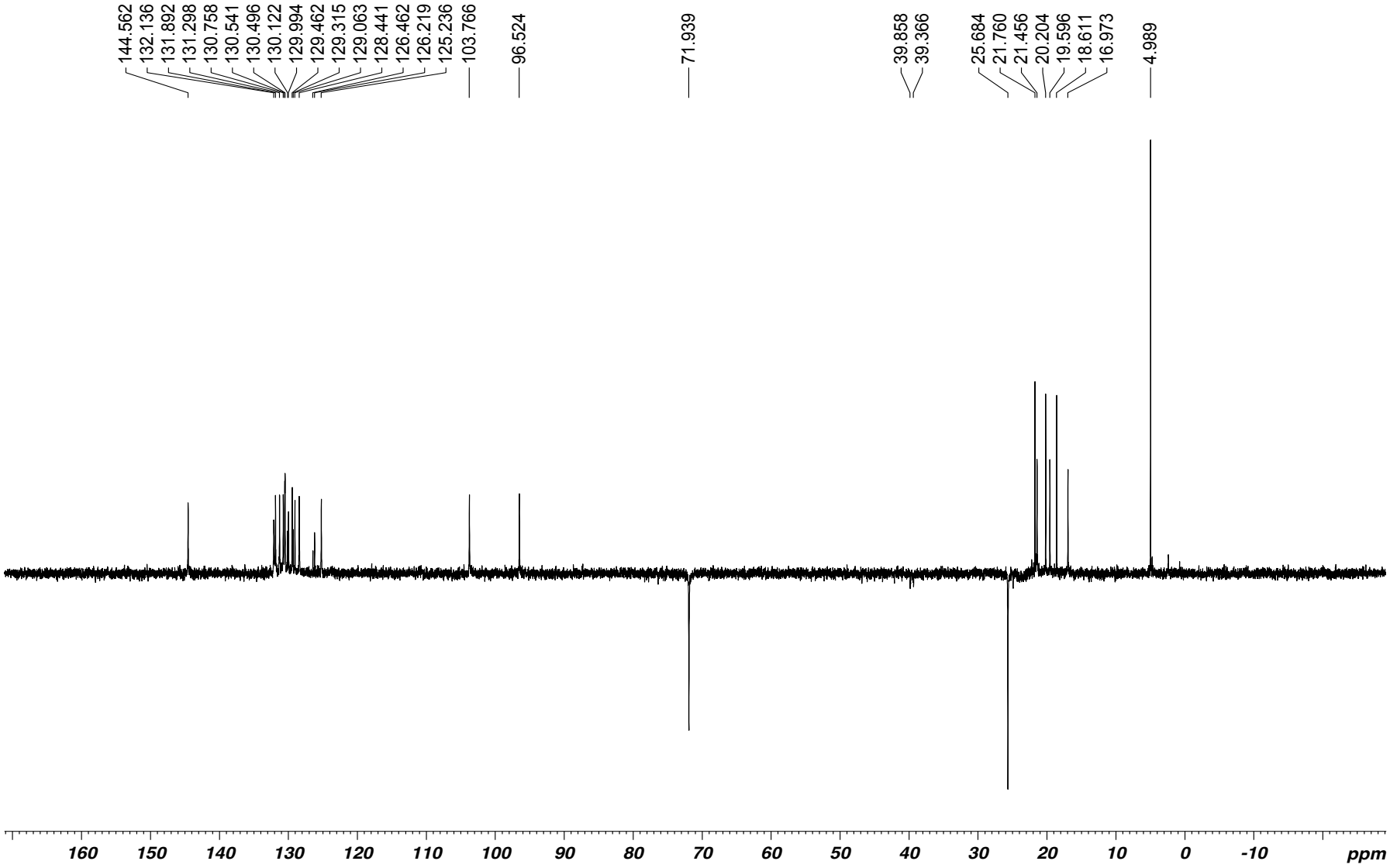

Figure S13. ^{13}C DEPT 135 NMR spectrum (100 MHz, toluene-d_8, 233 K) of the reaction product (3) of 2a' with 1 equiv of $B(C_6F_5)_3$.

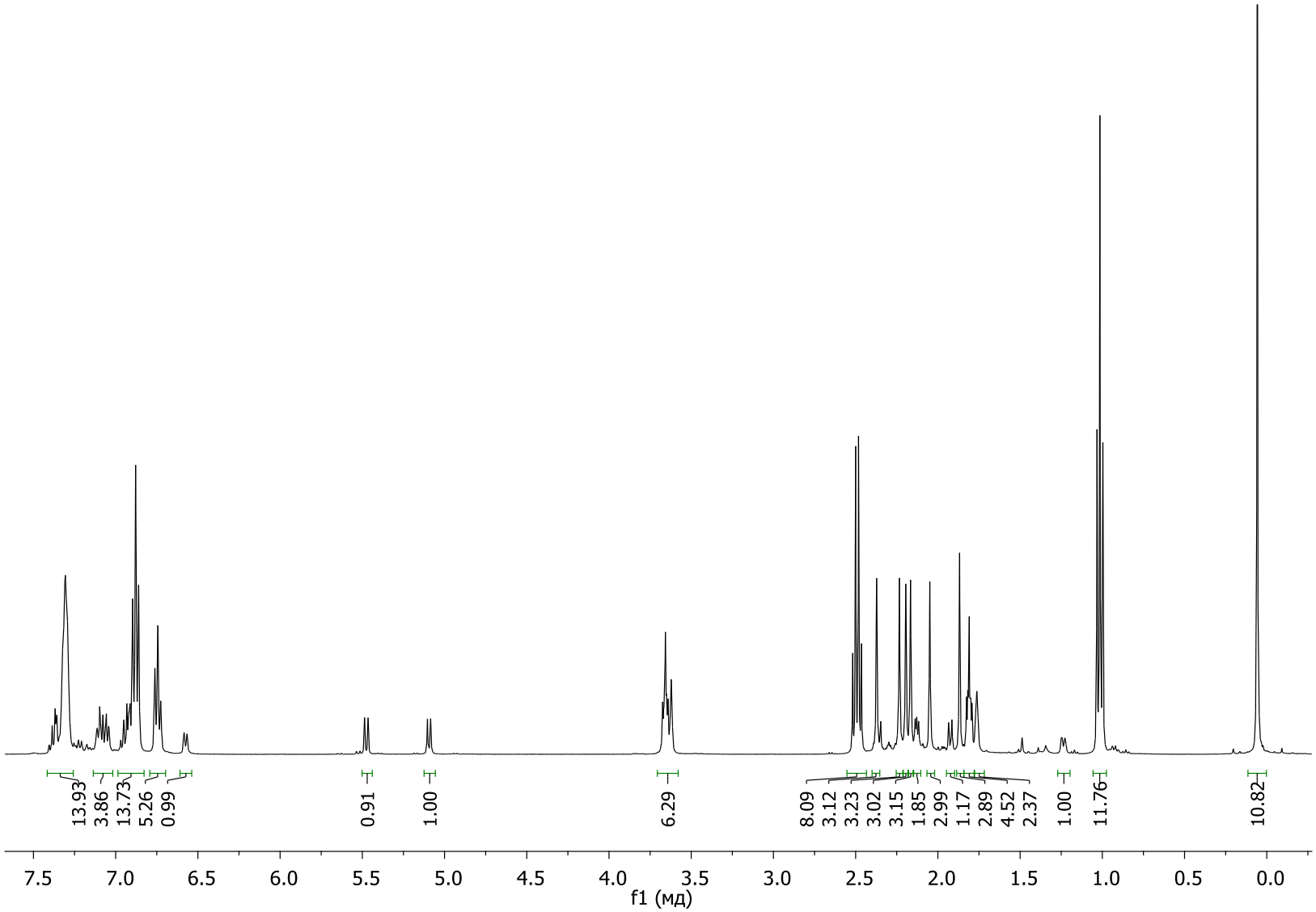

Figure S14. ^{1}H NMR spectrum (400 MHz, THF-d_8, 273 K) of the reaction product (4) of 2a' with 1 equiv of $[HNEt_3][BPh_4]$.

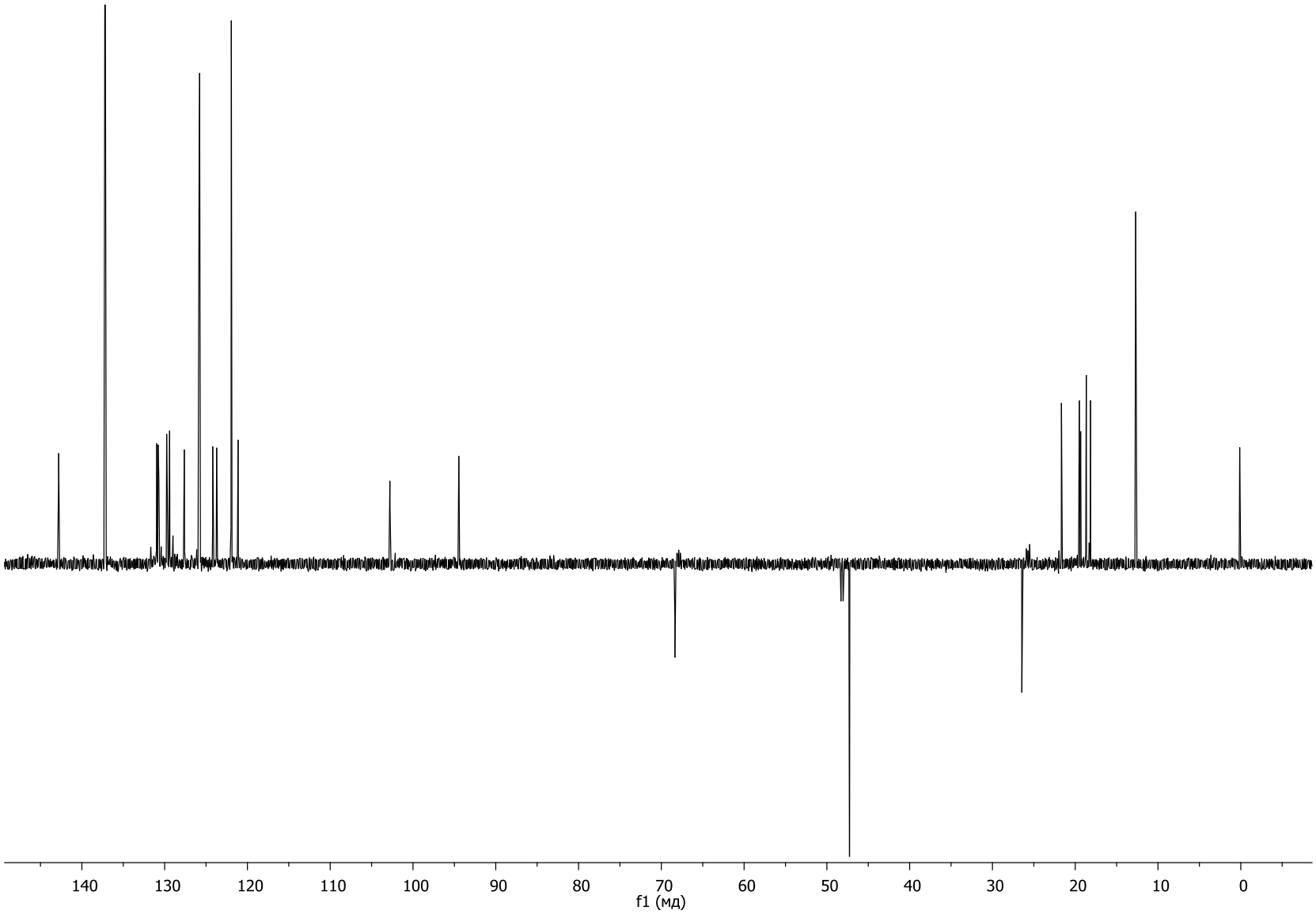

Figure S15. ^{13}C DEPT 135 NMR spectrum (400 MHz, THF-d_8, 273 K) of the reaction product (4) of 2a' with 1 equiv of $[HNEt_3][BPh_4]$.

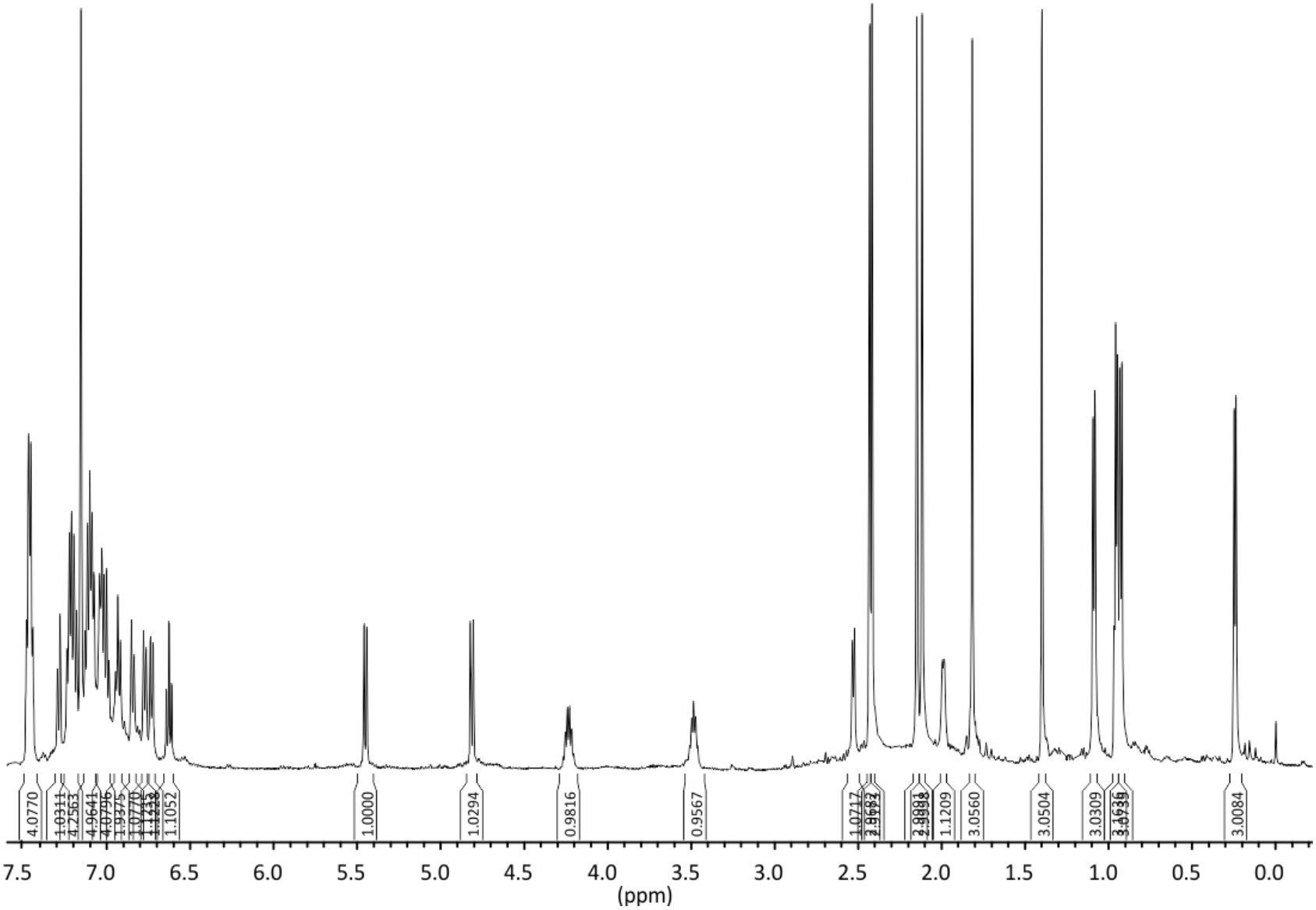

Figure S16. ^{1}H NMR spectrum (500 MHz, C_6D_6, 298 K) of the reaction product (5) of 2a' with 1 equiv of *i*PrN=C(PPh_2)-N(H)*i*Pr.

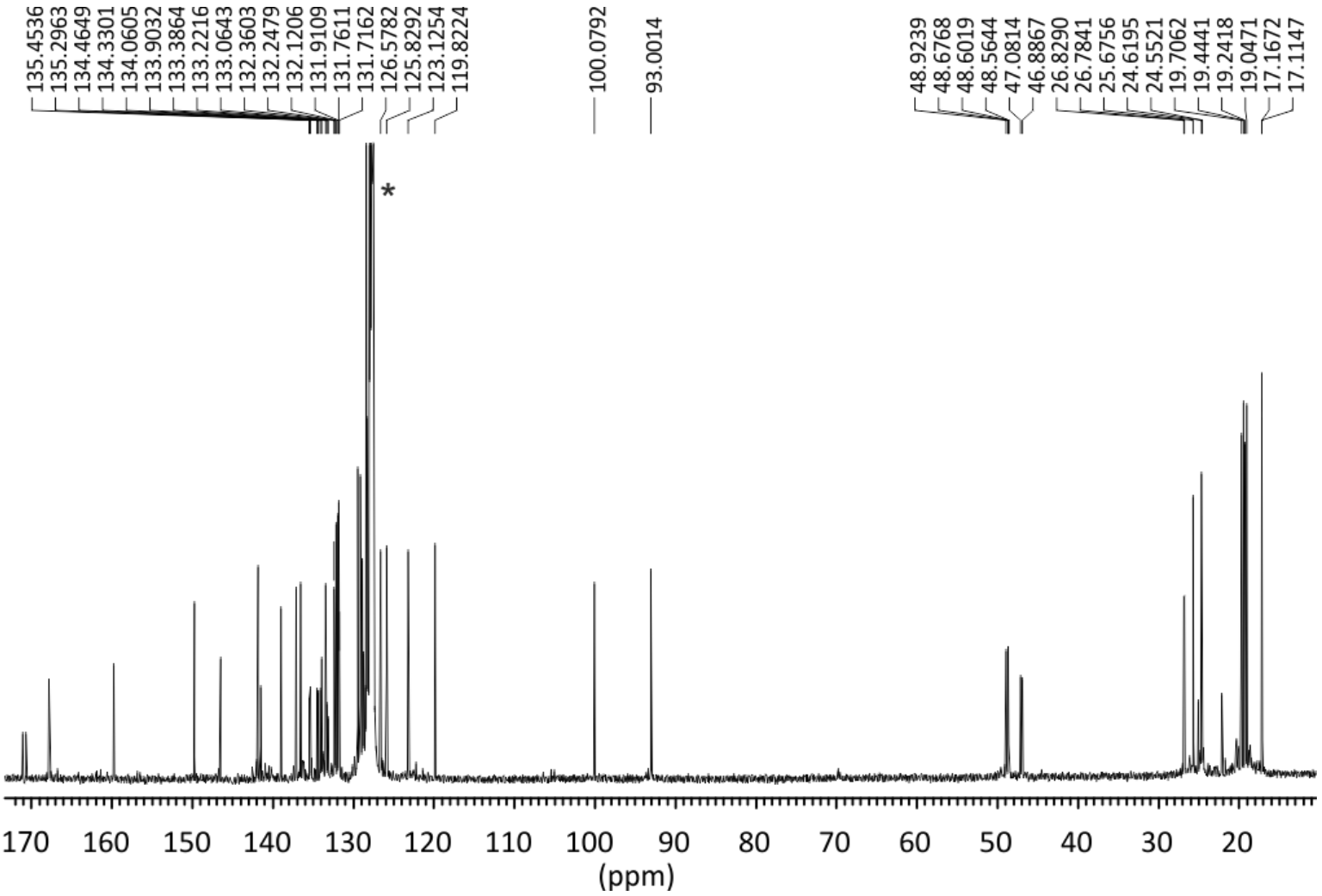

Figure S17. $^{13}C\{^{1}H\}$ NMR spectrum (125 MHz, C_6D_6, 298 K) of the reaction product (5) of 2a' with 1 equiv of *i*PrN=C(PPh_2)-N(H)*i*Pr. * stands for residual solvent signals.

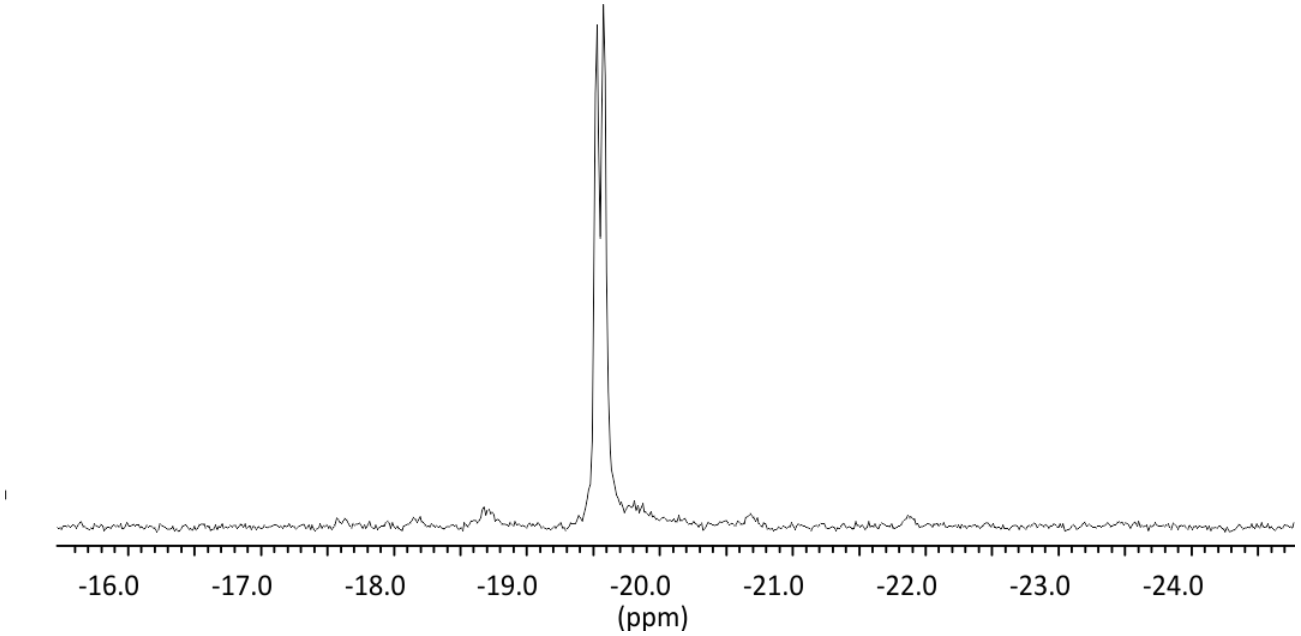

Figure S18. $^{31}P\{^{1}H\}$ NMR spectrum (121.5 MHz, C_6D_6, 298 K) of the reaction product (5) of 2a' with 1 equiv of *i*PrN=C(PPh_2)-N(H)*i*Pr.

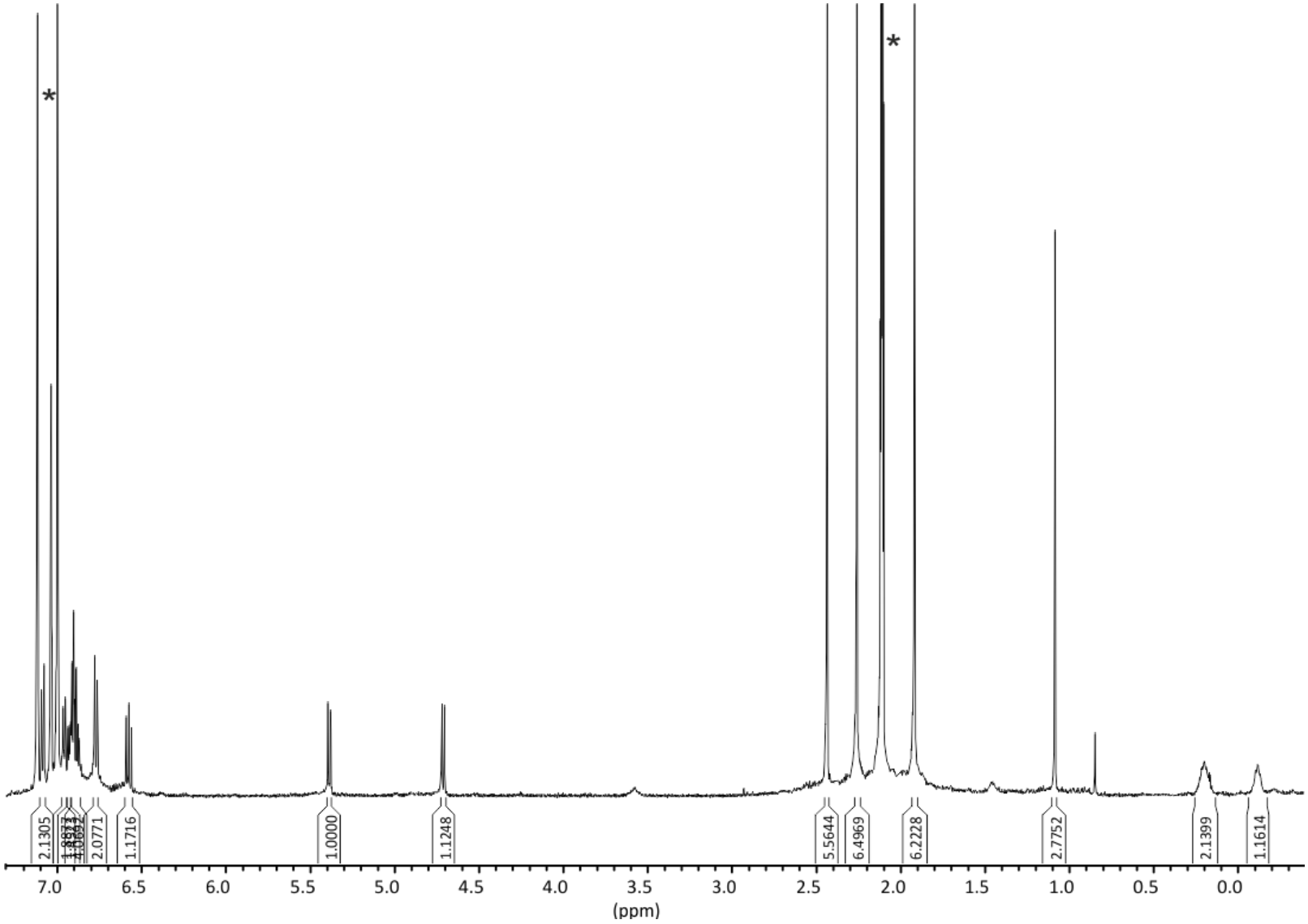

Figure S19. ^{1}H NMR spectrum (500 MHz, toluene-d_8, 298 K) of the reaction product (6) of 2a' with 1 equiv of NH_3BH_3. * stands for residual solvent signals.

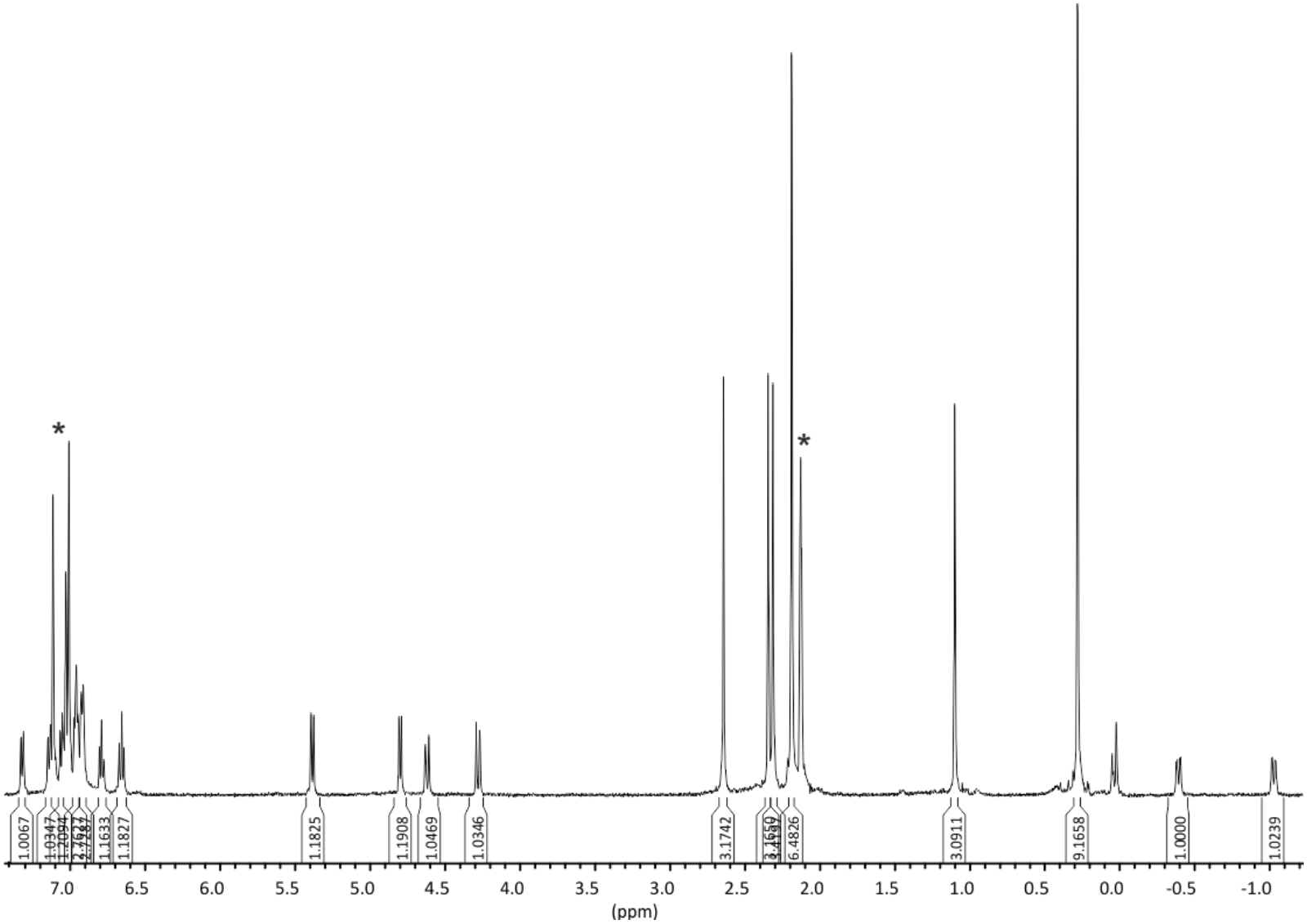

Figure S20. ^{1}H NMR spectrum (500 MHz, toluene-d_8, 333 K) of [{$N^{Me2}NN^{Me2}C^{Me}N^{Me}$–$CH_2$($\mu$-O)}Y($CH_2SiMe_3$)]$_2$ (7).* stands for residual solvent signals.

Table S1. Summary of crystal and refinement data for compounds 1, **2a'**, 6 and 7.

	1	**2a'**	6·toluene	7·toluene	7·(benzene)$_2$
Empirical formula	$C_{31}H_{34}N_4$	$C_{78}H_{102}N_8O_2Si_2Y_2$	$C_{38}H_{45}BN_5Y$	$C_{84}H_{102}N_8O_2Si_2Y_2$	$C_{70}H_{86}N_8O_2Si_2Y_2$, 2($C_6H_6$)
Formula weight	462.62	1417.68	671.51	1489.74	1461.68
Temperature, K	150(2)	250(2)	150(2)	150(2)	150(2)
Wavelength, Å	0.71073	0.71073	0.71073	0.71073	0.71073
Crystal system	Monoclinic	Monoclinic	Monoclinic	Monoclinic	Monoclinic
Space group	P 2_1/c	P 2_1/a	P 2_1/c	C 2/c	P 2_1/c
a, Å	17.8602(17)	14.061(3)	11.7059(4)	24.1225(15)	15.2617(5)
b, Å	7.5102(7)	18.161(3)	22.5039(6)	14.6664(7)	21.2573(5)
c, Å	21.248(2)	31.122(6)	13.3870(4)	29.2667(17)	24.7584(7)
Volume, Å^3	2591.9(4)	7798(3)	3419.67(18)	8837.8(9)	7696.7(4)
Z	4	4	4	4	4
Density (calc.), Mg/m^3	1.186	1.207	1.304	1.12	1.261
Absorption coefficient,mm^{-1}	0.070	1.559	1.739	1.379	1.582
Crystal size, mm^3	0.42 × 0.31 × 0.05	0.33 × 0.21 × 0.14	0.39 × 0.3 × 0.21	0.26 × 0.13 × 0.07	0.34 × 0.05 × 0.04
Reflections collected	19254	68336	27388	40414	71017
Independent reflections	5921	17751	7814	10106	17619
Data / restraints / parameters	5921 / 0 / 324	17751 / 0 / 835	7814 / 12 / 413	10106 / 0 / 452	17619 / 0 / 883
Final R indices [I>2σ(I)]	$R1$ = 0.0631, $wR2$ = 0.1465	$R1$ = 0.0622, $wR2$ = 0.1137	$R1$= 0.0433, $wR2$ = 0.0949	$R1$ = 0.0475, $wR2$ = 0.1146	$R1$ = 0.0621, $wR2$ = 0.105
R indices (all data)	$R1$ = 0.123, $wR2$ = 0.1738	$R1$ = 0.1964, $wR2$ = 0.149	$R1$= 0.0753, $wR2$ = 0.1056	$R1$ = 0.076, $wR2$ = 0.1241	$R1$ = 0.1556, $wR2$ = 0.1304
Goodness-of-fit on F^2	1.046	0.98	1.021	0.992	0.993
Largest diff. peak, e.Å^{-3}	0.232 and –0.242	0.494 and –0.345	0.484 and –0.566	0.72 and –0.442	0.67 and –0.619

Computational details. DFT calculations were carried out using the Gaussian 09 package,[1] employing B3LYP[2] and M06[3] functionals. Carbon, oxygen, nitrogen and hydrogen atoms were described with all-electron 6-31G(d,p) double-ζ quality basis sets.[4] Yttrium was represented by def2-TZVP, a triple-ζ valence basis set augmented by 2d1f polarization functions.[5] All stationary points were fully characterized via analytical frequency calculations as true minima (all positive eigenvalues). The optimized geometrical data for the molecules of **1** and **2a'**, obtained using M06 functional, were found in much better agreement with the X-ray crystallography results than those obtained with B3LYP method (Table S2). Therefore, M06 method was used for elucidating the bonding in the molecules of **1** and **2a'**. The electronic structures were studied by natural bond orbital (NBO) analysis.[6] Pictures of orbitals were generated using the program MOLEKEL 5.4.0.8.[7]

Table S2. Experimental (XRD) and calculated (M06, B3LYP) geometrical parameters and Wiberg bond indexes for **1** and **2a'**.

	1			**2a'**			
	Bond lengths (Å)		Wiberg bond index[b]	Bond lengths (Å)			Wiberg bond index[b]
	XRD	M06	-	XRD	B3LYP	M06	
Y(1)–C(1)	-	-	-	2.418(4)	2.441	2.417	0.4464
Y(1)–C(11)	-	-	-	2.475(4)	2.504	2.481	0.3543
Y(1)–C(12)	-	-	-	2.845(5)	2.945	2.848	0.0601
Y(1)–C(13)	-	-	-	2.907(5)	2.975	2.883	0.0542
Y(1)–N(1)	-	-	-	2.353(3)	2.402	2.378	0.2547
Y(1)–N(2)	-	-	-	2.344(3)	2.391	2.384	0.2109
Y(1)–N(4)	-	-	-	2.417(3)	2.454	2.412	0.1899
Y(1)–O(1)	-	-	-	2.389(3)	2.456	2.415	0.1705
C(2)–N(1)	1.373(3)	1.377	1.1248	1.343(5)	1.349	1.342	1.3021
C(2)–N(2)	1.347(3)	1.338	1.3327	1.378(5)	1.379	1.372	1.1806
C(3)–N(2)	1.337(3)	1.333	1.3627	1.338(5)	1.336	1.329	1.3195
C(3)–N(3)	1.406(3)	1.402	1.0344	1.434(5)	1.425	1.418	1.0179
C(4)–N(3)	1.406(3)	1.405	1.0266	1.388(6)	1.402	1.395	1.0982
C(4)–N(4)	1.276(3)	1.276	1.7518	1.280(5)	1.295	1.287	1.6089
	Bond angles (deg)			Bond angles (deg)			
	XRD	M06		XRD	B3LYP	M06	
N(1)–C(2)–N(2)	113.4(2)	114.9	-	110.8(3)	111.7	111.5	-
N(2)–C(3)–N(3)	114.6(2)	116.7	-	116.8(3)	118.8	118.5	-
N(3)–C(4)–N(4)	117.3(2)	117.6	-	121.6(4)	122.5	122.0	-
N(1)–Y(1)–C(1)	-	-	-	109.9(1)	116.3	115.2	-
Y(1)–C(11)–C(12)	-	-	-	89.4(3)	92.1	88.7	-
∠ N(1)–C(2)–N(2)–C(3)–N(3)-Me–N(3)–C(4)–N(4)	50.0(2)	51.8	-	21.4(4)	14.9	13.2	-

[b] M06 level

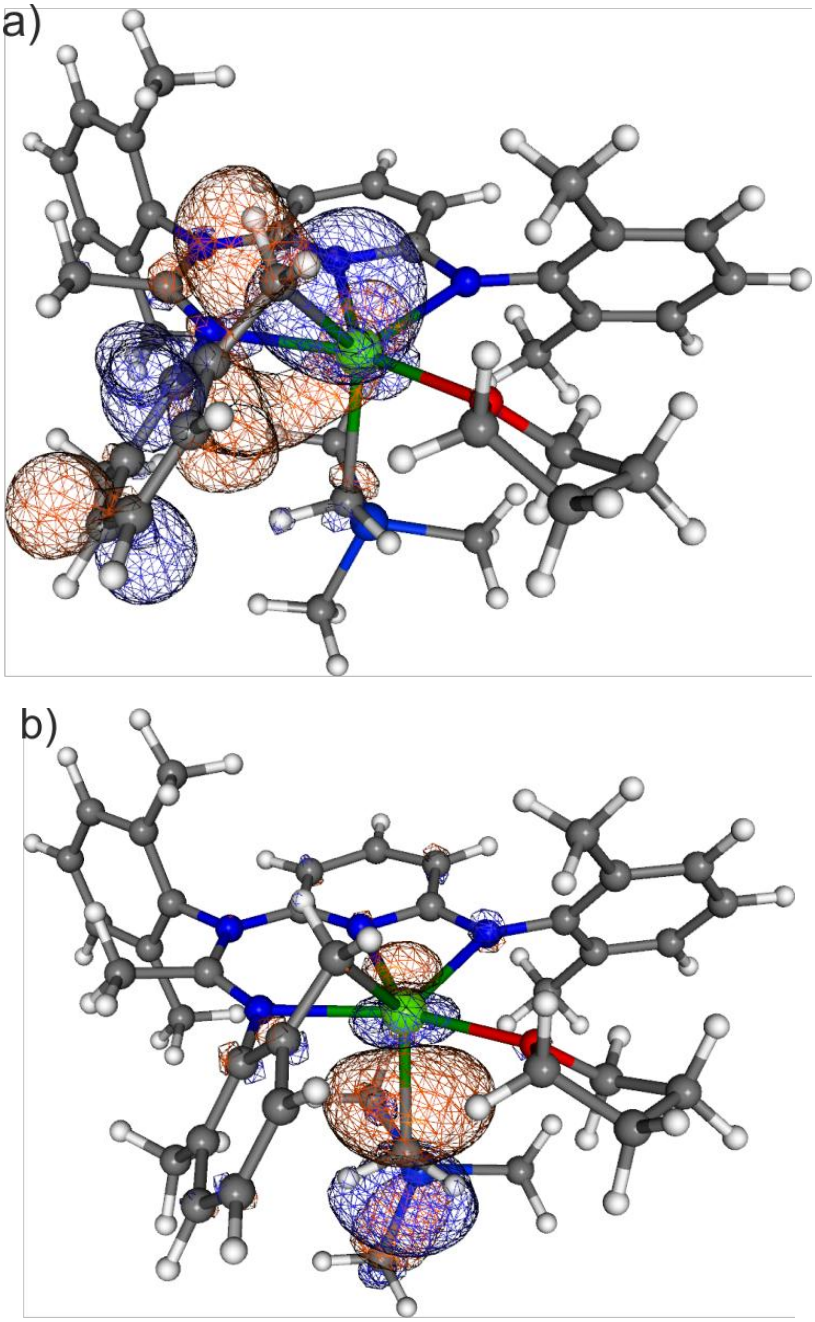

Figure S21. Kohn-Sham orbitals of **2a'** determined from M06 level calculations (isosurface value, 0.03): (a) HOMO (–0.1724 a.u.), (b) HOMO–1 (–0.1917 a.u.).

[1] Gaussian 09, Revision A.02, Frisch, M. J.; Trucks, G. W.; Schlegel, H. B.; Scuseria, G. E.; Robb, M. A.; Cheeseman, J. R.; Scalmani, G.; Barone, V.; Mennucci, B.; Petersson, G. A.; Nakatsuji, H.; Caricato, M.; Li, X.; Hratchian, H. P.; Izmaylov, A. F.; Bloino, J.; Zheng, G.; Sonnenberg, J. L.; Hada, M.; Ehara, M.; Toyota, K.; Fukuda, R.; Hasegawa, J.; Ishida,

M.; Nakajima, T.; Honda, Y.; Kitao, O.; Nakai, H.; Vreven, T.; Montgomery, Jr., J. A.; Peralta, J. E.; Ogliaro, F.; Bearpark, M.; Heyd, J. J.; Brothers, E.; Kudin, K. N.; Staroverov, V. N.; Kobayashi, R.; Normand, J.; Raghavachari, K.; Rendell, A.; Burant, J. C.; Iyengar, S. S.; Tomasi, J.; Cossi, M.; Rega, N.; Millam, J. M.; Klene, M.; Knox, J. E.; Cross, J. B.; Bakken, V.; Adamo, C.; Jaramillo, J.; Gomperts, R.; Stratmann, R. E.; Yazyev, O.; Austin, A. J.; Cammi, R.; Pomelli, C.; Ochterski, J. W.; Martin, R. L.; Morokuma, K.; Zakrzewski, V. G.; Voth, G. A.; Salvador, P.; Dannenberg, J. J.; Dapprich, S.; Daniels, A. D.; Farkas, Ц.; Foresman, J. B.; Ortiz, J. V.; Cioslowski, J.; Fox, D. J. Gaussian, Inc., Wallingford CT, 2009.

2 (a) Becke, A. D. *Phys. Rev. A* 1988, *38*, 3098. (b) Becke, A. D. *J. Chem. Phys.* 1993, *98*, 5648. (c) Lee, C.; Yang, W.; Parr, R. G. *Phys. Rev. B* 1988, *37*, 785.

3 Zhao, Y.; Schultz,N. E.;Truhlar,D. G. *J. Chem. Theo. Comput.* 2006, *2*, 364–82.

4 Hariharan, P. C.; Pople, J. A. *Theor.Chim.Acta* 1973, *28*, 213–222.

5 (a) Weigend, F.;Ahlrichs, R.*Phys. Chem. Chem. Phys.* 2005, *7*, 3297–3305. (b) Andrae, D.; Haeussermann, M.; Dolg, M.; Stoll, H.; Preuss, H. *Theor. Chim. Acta* 1990, *77*, 123–141.

6 Reed, A. E.; Curtiss, L. A.; Weinhold, F. *Chem. Rev.* 1988, *88*, 899–926.

7 Varetto, U. *MOLEKEL 5.4.0.8*; Swiss National Supercomputing Centre (CSCS): Lugano, Switzerland, 2009; http://www.cscs.ch.